Purification, Characterization, and Self-Assembly of the Polysaccharides from Allium Schoenoprasum

Fengrui Zhang
China Agricultural University
Jun Zheng
China Agricultural University
Zeyu Li
China Agricultural University
Zixuan Cai
China Agricultural University
Fengqiao Wang
China Agricultural University
Liubin Feng
Xiamen University - Malaysia
Dong Yang (dyang@cau.edu.cn)
China Agricultural University https://orcid.org/0000-0001-5435-5905

Research

Keywords: Chinese chive, Allium schoenoprasum, polysaccharide structure, hydrodynamic behavior, nanoparticle formation

Posted Date: July 6th, 2020

DOI: https://doi.org/10.21203/rs.3.rs-37389/v1

Abstract

Background: *Allium schoenoprasum is* a world-wide common vegetable while only its leave is used in the food factory. Its stalk is largely discarded, for potential heavy metal accumulations, which eventually lead to an environmental contamination. To fully utilize this vegetable and minimize its metal content, the major polysaccharide content is purified and characterized with chemical and computational approaches.

Results: The major polysaccharide component from the stalk of *Allium schoenoprasum* (*Ass*P) was extracted and purified. The gel filtration chromatography purified *Ass*P exhibited a molecular weight of around 1.6 kDa, which was verified by MALDI-ToF-MS. Monosaccharide analysis revealed its composition as rhamnose: arabinose: galactose: glucose: mannose: fructose with a molar ratio of 0.0264:2.46:3.71:3.35:1.00:9.93, respectively. Multiple NMR analysis revealed its backbone as α-Ara/Glu/Gal-(1→2)-linked and β-D-Fru-(4→5)-linked sugar residues. There was no tertiary structure of this polysaccharide, however, it self-assembled into a homogenous nanoparticle with a diameter of ~600 nm. The solution behavior of this *Ass*P polysaccharide was simulated, and there was no specific binding site on one molecule for another. Association of this polysaccharide was concentration dependent. As the *Ass*P concentration increased, the spherical particles increased their sizes and eventually merged into cylindrical micelles. The diversity of *Ass*P hydrodynamic behavior endowed potential versatility in its applications.

Conclusions: *Ass*P was characterized as a polysaccharide with identified monosaccharide compositions and linkage between them. Although there is no tertiary structure in one *Ass*P molecule, self-assembly of *Ass*P molecules could form nanoparticles or micelles depending on its solution concentrations. The unique *Ass*P solution behavior endows itself a potential biomaterial for nanoparticles preparations.

Background

Allium schoenoprasum, also known as Chinese chive, is a widely seen vegetable and seasoning on the dining table worldwide since ancient times. It was shown to exhibit antioxidant activity, with highest activity from its leaf of the cultivated plants and highest activity in its roots from the tissue culture plants[1-3]. The diallyl sulfide content in the chive oil inhibits a wide spectrum of foodborne pathogens, while the phenolic compounds, steroidal saponins, exhibited antiproliferative effects[4, 5]. Extracts from the chive leaves could inhibit Ehrlich carcinoma, and attenuates erythrocyte deformability in sickle cell anemia patients[6, 7]. However, it was also found that cadmium and selenium could accumulate in this plant to a toxic level[8-10].Thus, study on the extracts from *Allium schoenoprasum,* which could efficiently eliminate the heavy metal while maintains its biological function, became significant.

The stalk of the Chinese chive was shown to contain about 16% polysaccharides[11]. The structure of this polysaccharides purified from the *Allium schoenoprasum* stalk (*Ass*P) was preliminarily studied, and it showed an effect of reducing blood lipids of wistar rats[11]. More and more natural polysaccharides were investigated[12-16] and most of the studies were focusing on their biological functions while few reported their solution behaviors as encapsulating and delivering reagents. Here, we purified the polysaccharides from *A. schoenoprasum*, further studied its structure from primary to tertiary with different conclusions from previously reported, and its novel solution behavior both in the test tube and *in silico.* Results indicated this polysaccharide, with identified structures, could potentially server as a nanoparticle material in multiple circumstances.

Results

Extraction, purification, and molecular weight characterization of *Ass*P

Hot water was used to extract the polysaccharide from the stalk of the Chinese chive, and the crude polysaccharide was ethanol precipitated for its safety and simplicity for medicine and food products[17]. After pectin removal by $CaCl_2$ titration, the polysaccharide was dialyzed to remove small molecules. The polysaccharide was further purified with gel filtration chromatograph, and each fraction of elution was detected. In our experimental setup, *Ass*P eluted at around 270-330 mL with little impurities (Fig. 1, A).

Multiple methods were employed to measure the molecular weight of *Ass*P, including GPC and MALDI-TOF/TOF mass spectrometry. Firstly, polysaccharide molecular standard of pullulan with a variety of molecular weight (6600, 21700, 113000, 348000, 805000 Da) was loaded to a GPC column and each elution time was obtained. The log value of their molecular weight was plotted against each corresponding elution time and a standard curve with R^2 of 0.99 was obtained. The purified *Ass*P was analyzed with identical procedures, and its elution peak corresponding to a time range of 9.1-9.8 min centered at 9.35 min (Fig. 1, B). This corresponded to a molecular weight range of 3121-434 Da centered around 1543 Da. To further identify the molecular weight of *Ass*P, MALDI-TOF/TOF was employed to measure its accurate molecular weight. A cluster of peaks with 162 Da differences appeared on the mass spectrum in a range of 527.14-2147.38 Da, which is consistent with the GPC analysis (Fig. 1, C).

Structural characterization of *Ass*P

To determine the monosaccharide composition of *Ass*P, the polysaccharide was acid hydrolyzed before ion chromatography analysis. Monosaccharide standards of galactosamine, rhamnose, arabinose, galactose, glucose, mannose, fructose were analyzed in parallel to establish the curve for calculation of each mole fraction based on previous research[11]. The chromatogram of each above monosaccharide exhibited peak area that yielded a linear relationship with their concentrations that enabled us to calculate the corresponding mole fraction (Fig. 2, A, **Additional File 1:** Fig. S1, Table S1). Molar ratios of monosaccharides were calculated as 0.0264:2.46:3.71:3.35:1.00:9.93 of rhamnose: arabinose: galactose: glucose: mannose: fructose in the purified *Ass*P (Fig. 2, B). It is worthy to mention that in the previous study[11], the ratio of 5.1:22.6:31.5:1 as arabinose: galactose: glucose: mannose was obtained for *Ass*P. This is probably due to the incompetency of the 1-phenyl-3-methyl-5-pyrazolone (PMP)-derivation method they used for monosaccharide analysis, which could not detect the presence of fructose.

As shown in Fig. 3, A, the UV-Vis spectrum of gel filtration purified *Ass*P yielded a significant absorption at 192 nm while no absorbance at 260 or 280 nm, indicating non-detectable nucleotide or protein in the purified *Ass*P[18]. As shown in Fig. 3, B, functional groups of the *Ass*P were characterized with FT-IR. The strong and broad bands at ~3392 cm^{-1} indicates the hydroxyl (O–H) stretching vibration of the polysaccharide chain. Bands at 2932 cm^{-1} were ascribed to the asymmetric C–H stretching vibration. Absorption at 1644 cm^{-1} was assigned to the carbonyl stretching of the polysaccharide. The peak at 1416 cm^{-1} corresponded to the C=O stretching and C–O bond from the carboxyl group and C–H bending vibrations. The band at 1024 cm^{-1} corresponded to the C–OH bonds, and the band at 928 cm^{-1} corresponded to the asymmetric stretching of pyranose ring in the polysaccharide chain.

Integrative analysis of a variety of 1D and 2D NMR spectrums lead to the identification of chemical shifts of sugar residues and their possible glycosidic linkage as listed in Table 1. HSQC spectrum was applied to identify the anomeric carbons, COSY and H2BC spectroscopy were applied to identify the ^{1}H and ^{13}C chemical shift of adjacent sugar residues, while HMBC and HSQC-TOCSY spectroscopy were applied to further identify the ^{1}H and ^{13}C correlation in between sugar residues or within one sugar residue. A total of 4 anomeric carbons could be identified, indicating the presence of sugar residues in 4 different chemical environments. Residue a exhibited one less carbon than residues b, c, and d. Thus, residue a was designated as the arabinose residue, and identification of other sugar residue b, c, and d were listed in Table 1. Since the chemical shifts between b and c are not distinguishable, they were designated as the same sugar residue. As illustrated in the monosaccharide component analysis and ^{1}H spectroscopy (Fig. 4, A), sugar residues b and c should be galactose, and d should be glucose, respectively. In the one dimensional ^{13}C, (Fig. 4, B), there was 3 clusters of quaternary carbon signals at around 103 ppm, and these signals were correlated with residues a, b, c, and d. Combined with all the information, it was designated as the characteristic signals of fructose. With information from all the spectroscopy, fructose e, f, and g were identified and listed in Table 1.

The hydrocarbon coupling constants of anomeric carbons in residue a, b, c, and d were all around 170 Hz, indicating the presence of α-glycosidic bonds[19]. In the HMBC spectroscopy (Table 1), correlation signals were found between a1 and f2, b1 and f2, d1 and e2, c1 and e2, suggesting linkage between a(1→2)f, b(1→2)f, d(1→2)e, and c(1→2)e. In the NOESY spectroscopy (data not shown), correlation between b5, c5, d5 and f4, g4 were observed. With all the information, the main backbone of the purified *Ass*P could tentatively be α-L-Ara-(1→2)-β-D-Fru-(4→5)-α-D-G-(1→2)-β-D-Fru-(4→5)-α-D-G-(1→2)-β-D-Fru-(4→5)-α-D-G-(1→2)-β-D-Fru-(4→5)-α-D-G-(1→2)-β-D-Fru, among which G is Glc or Gal and the ratio between these two is approximately 1:1.

Tertiary structure and solution behavior of *Ass*P

Polysaccharides containing triple-helical structures form a Cong-red-polysaccharide complex, and the maximum absorption wavelength would have red-shifted compared with Congo-red solution. Addition of strong alkali disrupts the hydrogen bonding thus the red-shift of the Congo red-polysaccharide complex is weakened[20]. The tertiary structure of purified *Ass*P was examined with Cong red assay as shown in Fig. 5, A. The maximum absorption wavelength of the *Ass*P-Conge red mixture did not yield any dramatic change (491 to 489 nm) as the concentration of NaOH increased, indicating the absence of triple-helical structure of *Ass*P in solution.

The polysaccharide solution of each purification step was examined with DLS to reveal the solution behavior of *Ass*P at each stage (Fig. 5, B). Water extraction of the Chinese chive yielded a mixture of multiple-size polysaccharide solution, with particle size ranging from 100 nm to 5000 nm. After precipitation with ethanol, the large proportion of polysaccharide with size ranging from 100 to 500 nm were homogenized to ~300 nm, while the largest particle at ~5000 nm did not change. Removal of pectin further homogenized the polysaccharide solution to a ~150 nm size particle solution as indicated by the narrower peak. Notably, gel filtration which further purified *Ass*P rendered this polysaccharide to form a more homogenous, but larger size (with average size of ~600 nm) particle in solution. This was not mentioned in any studies previously, and it indicated a great potential of *Ass*P being used as a natural encapsulating/delivering reagent in the future.

The *Ass*P molecule in solution exhibited horseshoe-like configuration, and two *Ass*P clamped each other at their grooves (Fig. 6, A). The third polysaccharide molecule ended clamping to the first one, with no specific binding

site on neither of the *Ass*P molecules. Up to ten *Ass*P molecule were simulated to interact in solution. The fifth molecule joined the crowding by interacting with the third and the forth *Ass*P, with no direct interaction with the very first one. Aggregation of further more *Ass*P molecules exhibited a one-dimensional growth phenomenon where the binding of a later polysaccharide molecule always took place on the same site of the very first one. While stacking of these molecules yielded a certain curvature, nucleation at one side of the first *Ass*P molecule would certainly form a spherical structure.

To visualize the resulting scenario of *Ass*P aggregation, its solution state was simulated with sugar residues represented by coarse-grained bead to calculate their interactions (**Additional File 1:** Fig. S2, Table S2). This method emphasized on the solution distribution and particle formation (Fig. 6, B). At the very beginning of time (t=1step), the *Ass*P molecules distributed homogenously in the aqueous solution. As time passed (t=500 steps), the polysaccharide molecules aggregated into irregularly sized particles. Large spherical particles began to show up at a time point (t=3000 steps), and the system tended to favor this type of solution behavior where eventually all the *Ass*P molecules are distributed in the uniformly sized spherical particles (t=30000 steps). This is so far consistent with our DLS study (Fig. 5, B). However, it is likely a metastable state. At an approximate of infinite time point (t=50000 steps), the *Ass*P spherical particles began to disassembly into differently sized particles, suggesting an eventually unstable assembly of this polysaccharide nano-particle.

The solution particle was also concentration dependent as the equilibrium state (t=50000 steps) of different concentrations of *Ass*P were simulated (Fig. 6, C). At low concentrations, such as 1 mg/mL, the polysaccharide molecules form small spherical particles. As the concentration increased (10 mg/mL), the small particles approached each other and merged into larger particles. The spherical particles would merge into cylindrical micelle at higher *Ass*P concentrations (20 mg/mL), and the diameter of the cylinder would increase as the concentration further increased (30 mg/mL). The diversity of *Ass*P solution particle forms suggested a strong versatility in application.

Table 1 ^{13}C and ^{1}H NMR assignment for AssP.

Residue	Nucleus	Chemical shift (ppm)						HMBC	JCH(Hz)
		1	2	3	4	5	6		
a	^{1}H	5.34	3.44-3.44	3.68	3.36-3.40	3.74-3.77			
	^{13}C	92.42	71.12	72.49	69.18	59.79-60.29		a1-f2	171.2
b	^{1}H	5.33	3.44-3.45	3.67	3.41-3.47	3.83-3.87	3.70-3.74		
	^{13}C	92.2	71.02	72.45	69.12	70.90-71.81	59.90-60.59	b1-f2	170.2
c	^{1}H	5.32	3.46-3.47	3.66	3.36-3.40	3.84-3.87	3.74-3.77		
	^{13}C	92.13	71.04	72.4	69.12	71.17-71.72	59.79-60.29	c1-e2	168.4
d	^{1}H	5.31	3.47-3.48	3.65	3.41-3.47	3.83-3.87	3.70-3.74		
	^{13}C	91.95	70.97	72.38	69.11	70.90-71.81	59.90-60.59	d1-e2	168.5
e	^{1}H	3.58-3.61/3.65-3.69		4.08-4.11	3.98-4.02	3.76-3.81	3.6-3.75		
	^{13}C	59.98-60.67	103.62	76.32-76.91	74.06-74.55	81.25	62.23		
f	^{1}H	3.60-3.64/3.71-3.74		4.18-4.20	3.95-3.99	3.8	3.6-3.75		
	^{13}C	60.74-61.18	103.18	76.19-76.88	73.53-74.03	81.05	62.26		
g	^{1}H	3.78-3.81/3.62-3.65		4.12-4.16	4.03-4.07	3.75-3.80	3.6-3.75		
	^{13}C	60.29-61.03	102.98	77.07-77.83	74.00-74.57	81.05	61.75-62.58		

Discussion

Hot water extraction of polysaccharides from terrestrial plant has been the most efficient, low cost and environmental-friendly method in a variety of applications[21, 22]. One of the main purpose of this study is to remove potential heavy metal accumulation in this vegetable, thus careful use of edible chemical reagents were paid special attention through the purification steps. Size exclusion chromatography identified a single peak

after extraction steps as of water extraction, evaporation/concentration, ethanol precipitation, pH adjustment, calcium precipitation and dialysis. This comparatively simple set of purification steps suggests potential feasibility in industrial purification of *Ass*P.

The molecular weight, monosaccharide composition, and glycosidic linkages between sugar residues were identified. Unlike these more abundant polysaccharides from terrestrial biomass (e.g. xylans or cellulose) which has much larger molecular weights, *Ass*P is composed of only ~10 sugar residues[23, 24]. This of course contributes to the high solubility of *Ass*P in water. What is more, the monosaccharide composition in *Ass*P is more even while the glycosidic bonds are more diverse. Although there is no tertiary structure in *Ass*P, DLS experiments indicate that AssP eventually self-assembled into homogenous nanoparticles with a diameter of ~600 nm in solution. The particle size is not static but constantly changing during the purification steps, suggesting a concentration and time dependent solution behavior of *Ass*P. Simulation results indicate that association of *Ass*P molecules in solution exhibit a non-specific manner where binding of one molecule to the other one is not at a certain sugar residue. Meanwhile, there is a certain pattern of *Ass*P molecule association that the later associating molecules always binds to the complex from the same side and form a curvature. As more and more molecules associated, this curvature eventually end up as a spherical nanoparticle. More interestingly, *Ass*P form spherical nanoparticles at concentration of 10 mg/mL and lower or micelles at concentration of 20 mg/mL and higher. This phenomenon of concentration dependent nanoparticle formation was reported with polyelectrolyte complex dispersions (PECs) formed nanoparticles[25]. However, it is rarely seen in biomass-based nanoparticles.

Biopolymeric nanoparticles are often categorized into polysaccharide nanoparticles and protein nanoparticles, which all find applications in drug delivery in controlled or sustained or targeted manner[26]. Nanoparticles made from carbohydrates or polysaccharide played a wide role in pharmaceutical industry due to their excellent biocompatibility, which are often used to deliver proteins, peptides and nucleic acids[27-29]. Fabrication of biomass-based nanoparticles often involves a variety of technique including desolvation, coacervation, emulsification-diffusion and electrohydrodynamic atomization. *Ass*P could self-assembly into either spherical nanoparticles or micelles at different diameters with fine tune of solution concentrations without the above mentioned fabrication process. This is, to the best of our knowledge, not reported previously and suggesting a promising application of *Ass*P as a self-assembly biomaterial of nanoparticles for different scenario.

Conclusions

The major polysaccharide component of a tradition vegetable *Allium schoenoprasum* was purified and characterized. Different from the previous report, our study revealed a monosaccharide composition of this *Ass*P was arabinose: galactose: glucose: fructose of approximately 1:2:2:5. The main backbone of this polysaccharide is α-Ara/Glu/Gal-(1→2)-linked and ß-D-Fru-(4→5)-linked sugar residues, and it forms ~600 nm nanoparticles in water solution. *Ass*P exhibited concentration dependence in forming different solution assemblies, and this behavior diversity could serve in different applications.

Methods

Materials and chemicals

Air dried *A. schoenoprasum* stalk was kindly offered by Jiangsu Natural Food Co., Ltd. (Xinghua, Jiangsu Province, China). Calcium chloride dehydrate, absolute ethanol, sulfuric acid and aqueous ammonia of analytic grade were purchased from Beijing Chemical Works (Beijing, China).

Extraction and purification of *Ass*P

Purification of chive polysaccharides was following the methods developed by Zhang Y [11] with modification. The grinded, dry chive stalk was filtered through a 20 mesh screen, rinsed with 30-folds (by weight) of water for 2 hours at 85 ℃. The residue was removed with gauze, and filtrated to get clear solution before further concentrated with a rotary evaporator (RE-200, Yarong Biochemical Instrument, Shanghai, China). Addition of 4-folds (by volume) of anhydrous ethanol was performed to precipitate the polysaccharides overnight. After removal of the supernatant, the polysaccharide was resuspended in water and ammonia solution was added to adjust the pH to 8.5. Then 10% calcium chloride solution was titrated until white precipitation appears in the solution. The solution was centrifuged to remove the pectin precipitation, and the titration was repeated until no more precipitation was seen. The solution was then loaded into a dialysis bag with molecular cutoff of 500Da, dialyzed against water 6 times at 4 ℃ for a total of 48 hours. The *Ass*P solution was then concentrated, filtered through a 0.22 μM filter and purified on a HiPrep^{TM} Sephacryl^{TM} S-400 HR gel filtration chromatography column (GE Healthcare, USA). The flow rate of water was set at 1 mL/min and every 5 mL of elution was collected. The polysaccharide content in each elution was monitored by measuring its absorbance at 200 nm on a DS-11 FX+ spectrophotometer (DeNovix, Wilmington, DE, USA). The polysaccharide concentration was measured with the phenol-sulfuric acid method as previously[20].

Gel permeation chromatography

The purified *Ass*P of 1 mg/mL was analyzed with a PL aquagel-OH Mixed-H GPC/SEC column (300×7.5mm, Agilent) on a 1260 Infinity II GPC/SEC system coupled with a G7800A refractive index detector. The mobile phase contains pure water which was set at a flow rate of 1.0 mL/min and the column was incubated at 30℃. Polysaccharides GPC standards analyzed in parallel are pullulan or polymaltotriose with molecular weights of 6600, 21700, 113000, 348000, 805000 Da (ZZBio Co., LTD, Shanghai, China).

Mass spectroscopy

The *Ass*P sample was mixed in equal volume with 2,3-dihydroxybenzoic acid (DHB) and spotted onto a MALDI target pre-spotted with 5-chloro-2-mercaptobenzothiazole (CMBT). After air drying, crystallized spots were detected with a MALDI-TOF/TOF mass spectrometry (AB SCIEX 5800, AB Sciex, CA, USA). Polysaccharide mass maps were acquired in the positive reflectron mode with an accelerating voltage set at 20 kV. Spectra were obtained by accumulating 3500 laser shots for quantification with the laser intensity set at 6659. Calibration mixtures were used to calibrate the spectrum.

Monosaccharide composition analysis

*Ass*P was totally hydrolyzed with equal volume of 0.4 mol/L trifluoroactic acid (TFA) at 110 ℃ for 2 hours in a sealed glass tube. The hydrolysate was dried under reduced pressure at a temperature lower than 40 ℃. The same volume of ethanol was added to the dry hydrolysate to dissolve residual TFA and evaporated under the above condition. This was repeated 3 times to scavenge TFA. The dried hydrolysate was dissolved in 1 mL of

ultrapure water and stored at 4 ℃ for later use. The monosaccharide standard was made to 1μg/mL solutions. Both the *Ass*P hydrolysate and the monosaccharide standard were filtered with a 0.22 μm membrane filter before analyzed on a Dionex CarboPac PA10 analytical column (250mm×4mm, Thermo Scientific) installed on a Dionex ICS-5000^{+} ion chromatography System coupled with a DC detector (Thermo Scientific). The mobile phase contains a mixture of 80:20 (v:v) of water and 250 mM/L NaOH with a flowrate of 1.0 mL/min. The molar ratio of the monosaccharide component was calculated by area via the standard curve established with pure monosaccharide of known concentrations.

UV-Vis spectroscopy

The UV-Vis spectra of *Ass*P (0.25 mg/mL) was recorded on a Hitachi U-3900H spectrophotometer (Tokyo, Japan) in a quartz cuvette with a light path of 1 cm. The absorbance was recorded between 190 and 800 nm with a step size of 1 nm.

FT-IR spectroscopy

FT-IR spectra of *Ass*P was recorded on a PerkinElmer FT-IR spectrometer (Spectrum 100, Fremont, USA). An aliquot of 5.0 mg freeze-dried *Ass*P was blended with 200 mg potassium bromide into powder and pressed into pellets. The sample was scanned at room temperature under dry air, and 16 scans of the transmittance were recorded between 4000 and 452 cm^{-1} with a step size of 4 cm^{-1}. The collected spectra was processed with Spectrum 10 software(PerkinElmer).

Nuclear magnetic resonance

The *Ass*P was dissolved in 3% (w/w) D_2O and incubated for 3 hours before the solution was freeze-dried. This step was repeated three times. The deuterated *Ass*P was dissolved again in D_2O of about 100 mg/ml for NMR measurement. All NMR spectra were acquired at 850 (^{1}H) or 212 MHz (^{13}C) on a Bruker NMR instrument 850 MHZ spectrometer using 5mm CPTCI probe at 27 °C. One-dimensional proton, ^{13}C and two-dimensional COSY, edit-HSQC, HSQC-TOCSY, NOESY, HMBC and H2BC spectra were acquired. 1-D proton spectrum was averaged from 16 scans, and 1-D ^{13}C spectrum was acquired in 2048 scans. The 2-D COSY spectra were acquired in 4 scans per increment and 256 increments, the edit-HSQC spectra in 8 scans and 256 increments, the HSQC-TOCSY spectra in 16 scans per increment and 256 increments, the NOESY spectra in 8 scans per increment and 256 increments, and the HMBC spectra in 32 scans and 128 increments. The relaxation delays for the NMR experiments were 2s. Mixing time for the TOCSY and NOESY spectra were 80 and 300ms, respectively.

Dynamic light scattering

Particle size of the *Ass*P was determined with a dynamic light scattering (DLS) instrument (Zetasizer Nano-ZS90, Malvern Instruments Ltd., Worcestershire, UK), and the measurement was carried out at 25℃. The particle size was calculated by the Stokes-Einstein equation and reported as a cumulative mean diameter (size, nm) for size distribution[30].

Congo red test

The tertiary conformation of *Ass*P was analyzed by the interaction with Cong red. Briefly, 2 mg polysaccharide sample was mixed with 2 mL distilled water and 2 mL Congo red solution (80 μmol/L). Different volumes of NaOH solution (1 mol/L) were added to the mixture gradually to obtain the final NaOH concentration of 0-0.5 mol/L. The mixed solution without polysaccharides was scanned as a control. The maximum absorption wavelength at different concentrations of NaOH solution were determined in the range of 200-600 nm after equilibration at room temperature for 10 min[31].

Molecular interaction simulation

Discovery Studio v16 (BIOVIA, USA) was employed to perform the molecular simulation of interactions between *Ass*P molecules with the CDOCKER molecular docking model. The 3D molecular structure of *Ass*p was created in a new molecule window, and the CHARMm force field was added before the Standard Dynamics Cascade was conducted [32]. The oligosaccharide conformation with the lowest total energy was selected and water molecules were removed to prepare the acceptor molecule file. The whole *Ass*P molecule was selected as the binding site while another *Ass*p molecule added as the ligand to conduct the CDOCKER simulation. After the first round of simulation, the optimized *Ass*P dimer was conceived as the receptor and a third *Ass*p molecule was introduced as the ligand to perform the next round of CDOCKER simulation. The above steps were repeated until the 10^{th} *Ass*p molecule was introduced into the complex.

Hydrodynamic behavior simulation

The dissipative particle dynamics (DPD), a mesoscopic scale simulation technique, was employed to simulate the hydrodynamic behavior of *Ass*P molecules in aqueous solution. Coarse-Graining models was used to represent the *Ass*P and water molecules. For *Ass*p, the coarse-grained structure is $AF(GF)_4$, where bead A, F and G represents arabinoside, fructoside and glucoside/galactoside, respectively. Bead W represent water molecule. The Flory-Huggins parameters (x_{ij}) between component i and j were determined by approximation with solubility parameter δ_i with the following formula[33]:

$$\chi_{ij} = \frac{V([\delta_i] - \delta_j)^2}{RT}$$

where V is the arithmetic average of the molar volumes of components i an j. δ_i and δ_j are the solubility parameters of components i and j, respectively. R is the ideal gas constant and T (K) is the temperature of the system.

The solubility parameters of each component was calculated by the Amorphous Cell modules. The 3D structure of each component was constructed and energy minimized with the Minimizer in the Discover module. The *Ass*P system was constructed with the Construction function in the Amorphous Cell module, and energy minimized with the Discover module. The Dynamics function in the Discover module was employed to calculate the system density which was then used to construct the *Ass*P system again. Once the latest polysaccharide system was energy minimized, the final density was used to calculate the solubility parameter with the Analysis in the Amorphous Cell module. Calculation of the repulsion parameters (a_{ij}) between component i and j were determined by the Flory-Huggins parameter x_{ij} with the following formula[34]:

$$a_{ij} = 25 + 3.27\chi_{ij}, \rho = 3$$

To perform the DPD Simulation, a cubic simulation box with 30×30×30 R^3c side lengths was constructed. The Default spring constant between the beads was set to 4.0, and the time step was set 0.05. The PDP simulation was carried out with the DPD module implemented in MS.

Abbreviations

Ara: arabinose

CMBT: 5-chloro-2-mercaptobenzothiazole

COSY: Correlation spectroscopy

DHB: 2,3-dihydroxybenzoic acid

DLS: dynamic light scattering

Fru: fructose

Gal: galactose

Glc: glucose

GPC: gel permeation chromatography

H2BC: Heteronuclear 2-bond correlation

HMBC: Heteronuclear multiple bond correlation

HSQC: Heteronuclear single-quantum correlation

MALDI-ToF-MS: Matrix assisted laser desorption ionization-time of fly-mass spectrometry

NMR: nuclear magnetic resonance

NOESY: Nuclear overhauser effect spectroscopy

PMP: 1-phenyl-3-methyl-5-pyrazolone

SEC: size exclusion chromatography

TFA: trifluoroactic acid

TOCSY: Total correlation spectroscopy

Declarations

Ethics declarations

Ethics approval and consent to participate

Not applicable

Consent for publication

All authors have seen and approved the manuscript before submission to Biotechnology for Biofuels.

Competing interests

The authors declare no conflicts of interest.

Fundings

This work was supported by the National Key Research and Development Program of China (2019YFC1605000), National Laboratory of Biomacromolecules (2018kf09), the “Shuang Chuang” Plan of Taizhou City, Jiangsu Province, and the Xinghua Industrial Research Centre for Food Science and Human Health, China Agricultural University.

Authors’ contributions

DY conceived the study. FZ, JZ, ZL, ZC, FW and LF performed the experiments. DY and LF analyzed the data. DY wrote the manuscript. All authors read and approved the final manuscript.

Acknowledgements

The authors are grateful to Prof. Zhanhui Wang for help in the software of molecular simulation work and Prof. Chih-chen Wang in the Institute of Biophysics, Chinese Academy of Sciences for her support and encouragement in our research. The authors declare no conflict of interest.

Availability of data and materials

The datasets used during this study are available from the corresponding author upon request.

References

1. Stajner D, Canadanovic-Brunet J, Pavlovic A: Allium schoenoprasum L., as a natural antioxidant. Phytother Res 2004; 18:522-524.
2. Stajner D, Popovic BM, Calic-Dragosavac D, Malencic D, Zdravkovic-Korac S: Comparative study on Allium schoenoprasum cultivated plant and Allium schoenoprasum tissue culture organs antioxidant status. Phytother Res 2011; 25:1618-1622.
3. Bezmaternykh KV, Shirshova TI, Beshlei IV, Matistov NV, Smirnova GV, Oktyabr'skii ON, Volodin VV: Antioxidant Activity of Extracts from Allium Schoenoprasum L. and Rubus Chamaemorus L. Growing in the Komi Republic. Pharmaceutical Chemistry Journal 2014; 48:116-120.
4. Kucekova Z, Mlcek J, Humpolicek P, Rop O, Valasek P, Saha P: Phenolic compounds from Allium schoenoprasum, Tragopogon pratensis and Rumex acetosa and their antiproliferative effects. Molecules 2011; 16:9207-9217.

5. Timite G, Mitaine-Offer AC, Miyamoto T, Tanaka C, Mirjolet JF, Duchamp O, Lacaille-Dubois MA: Structure and cytotoxicity of steroidal glycosides from Allium schoenoprasum. Phytochemistry 2013; 88:61-66.
6. Shirshova TI, Beshlei IV, Deryagina VP, Ryzhova NI, Matistov NV: Chemical composition of Allium schoenoprasum leaves and inhibitory effect of their extract on tumor growth in mice. Pharmaceutical Chemistry Journal 2013; 46:672-675.
7. Shirshova TI, Beshlei IV, Deryagina VP, Ryzhova NI: The Component Composition of Steroid Glycosides Extracted from the Fruits of Allium Schoenoprasum L. and Assessment of Their Effects on the Growth of Transplanted Tumors in Mice. Pharmaceutical Chemistry Journal 2014; 48:328-331.
8. Barazani O, Dudai N, Khadka UR, Golan-Goldhirsh A: Cadmium accumulation in Allium schoenoprasum L. grown in an aqueous medium. Chemosphere 2004; 57:1213-1218.
9. Kapolna E, Fodor P: Bioavailability of selenium from selenium-enriched green onions (Allium fistulosum) and chives (Allium schoenoprasum) after 'in vitro' gastrointestinal digestion. Int J Food Sci Nutr 2007; 58:282-296.
10. Eisazadeh S, Asadi Kapourchal S, Homaee M, Noorhosseini SA, Damalas CA: Chive (Allium schoenoprasum L.) response as a phytoextraction plant in cadmium-contaminated soils. Environ Sci Pollut Res Int 2019; 26:152-160.
11. Zhang Y: Study on extraction, purification and biological activity of fistular onion stalk (Allium schoenoprasum L.) polysaccharides**.** *Master:* Nanjing Agricultural University, 2009.
12. Chen Y, Mao W, Wang B, Zhou L, Gu Q, Chen Y, Zhao C, Li N, Wang C, Shan J, et al: Preparation and characterization of an extracellular polysaccharide produced by the deep-sea fungus Penicillium griseofulvum. Bioresour Technol 2013; 132:178-181.
13. Goo BG, Baek G, Choi DJ, Park YI, Synytsya A, Bleha R, Seong DH, Lee CG, Park JK: Characterization of a renewable extracellular polysaccharide from defatted microalgae Dunaliella tertiolecta. Bioresour Technol 2013; 129:343-350.
14. Tong H, Xia F, Feng K, Sun G, Gao X, Sun L, Jiang R, Tian D, Sun X: Structural characterization and in vitro antitumor activity of a novel polysaccharide isolated from the fruiting bodies of Pleurotus ostreatus. Bioresour Technol 2009; 100:1682-1686.
15. Sun Y, Liang H, Zhang X, Tong H, Liu J: Structural elucidation and immunological activity of a polysaccharide from the fruiting body of Armillaria mellea. Bioresour Technol 2009; 100:1860-1863.
16. Rout S, Banerjee R: Free radical scavenging, anti-glycation and tyrosinase inhibition properties of a polysaccharide fraction isolated from the rind from Punica granatum. Bioresour Technol 2007; 98:3159-3163.
17. Golunski S, Astolfi V, Carniel N, de Oliveira D, Di Luccio M, Mazutti MA, Treichel H: Ethanol precipitation and ultrafiltration of inulinases from Kluyveromyces marxianus. Separation and Purification Technology 2011; 78:261-265.
18. Yan JK, Wang YY, Qiu WY, Shao N: Three-phase partitioning for efficient extraction and separation of polysaccharides from Corbicula fluminea. Carbohydr Polym 2017; 163:10-19.
19. Snyder JR, Serianni AS: D-Idose - a One-Dimensional and Two-Dimensional Nmr Investigation of Solution Composition and Conformation. Journal of Organic Chemistry 1986; 51:2694-2702.

20. Yu P, Zhou F, Yang D: Curdlan conformation change during its hydrolysis by multi-domain beta-1,3-glucanases. Food Chem 2019; 287:20-27.
21. Liu Q, Yao C, Sun Y, Chen W, Tan H, Cao X, Xue S, Yin H: Production and structural characterization of a new type of polysaccharide from nitrogen-limited Arthrospira platensis cultivated in outdoor industrial-scale open raceway ponds. Biotechnol Biofuels 2019; 12:131.
22. Luo X, Liu J, Zheng P, Li M, Zhou Y, Huang L, Chen L, Shuai L: Promoting enzymatic hydrolysis of lignocellulosic biomass by inexpensive soy protein. Biotechnol Biofuels 2019; 12:51.
23. Smith PJ, Wang HT, York WS, Pena MJ, Urbanowicz BR: Designer biomass for next-generation biorefineries: leveraging recent insights into xylan structure and biosynthesis. Biotechnol Biofuels 2017; 10:286.
24. Zeng Y, Himmel ME, Ding SY: Visualizing chemical functionality in plant cell walls. Biotechnol Biofuels 2017; 10:263.
25. Hartig SM, Greene RR, DasGupta J, Carlesso G, Dikov MM, Prokop A, Davidson JM: Multifunctional nanoparticulate polyelectrolyte complexes. Pharm Res 2007; 24:2353-2369.
26. Verma ML, Dhanya BS, Sukriti, Rani V, Thakur M, Jeslin J, Kushwaha R: Carbohydrate and protein based biopolymeric nanoparticles: Current status and biotechnological applications. Int J Biol Macromol 2020; 154:390-412.
27. Rajaonarivony M, Vauthier C, Couarraze G, Puisieux F, Couvreur P: Development of a New Drug Carrier Made from Alginate. Journal of Pharmaceutical Sciences 1993; 82:912-917.
28. Wang N, Wu XS: Preparation and characterization of agarose hydrogel nanoparticles for protein and peptide drug delivery. Pharm Dev Technol 1997; 2:135-142.
29. Calvo P, RemunanLopez C, VilaJato JL, Alonso MJ: Novel hydrophilic chitosan-polyethylene oxide nanoparticles as protein carriers. Journal of Applied Polymer Science 1997; 63:125-132.
30. Chen S, Han Y, Sun C, Dai L, Yang S, Wei Y, Mao L, Yuan F, Gao Y: Effect of molecular weight of hyaluronan on zein-based nanoparticles: Fabrication, structural characterization and delivery of curcumin. Carbohydr Polym 2018; 201:599-607.
31. Cao JJ, Lv QQ, Zhang B, Chen HQ: Structural characterization and hepatoprotective activities of polysaccharides from the leaves of Toona sinensis (A. Juss) Roem. Carbohydr Polym 2019; 212:89-101.
32. Brooks BR, Bruccoleri RE, Olafson BD, States DJ, Swaminathan S, Karplus M: CHARMM - A program for macromolecular energy, minimization, and dynamics calculatoins. Journal of Computational Chemistry 1983; 4:187-217.
33. Zhao Y, You LY, Lu ZY, Sun CC: Dissipative particle dynamics study on the multicompartment micelles self-assembled from the mixture of diblock copolymer poly(ethyl ethylene)-block-poly(ethylene oxide) and homopolymer poly(propylene oxide) in aqueous solution. Polymer 2009; 50:5333-5340.
34. Groot RD, Warren PB: Dissipative particle dynamics: Bridging the gap between atomistic and mesoscopic simulation. Journal of Chemical Physics 1997; 107:4423-4435.

Figures

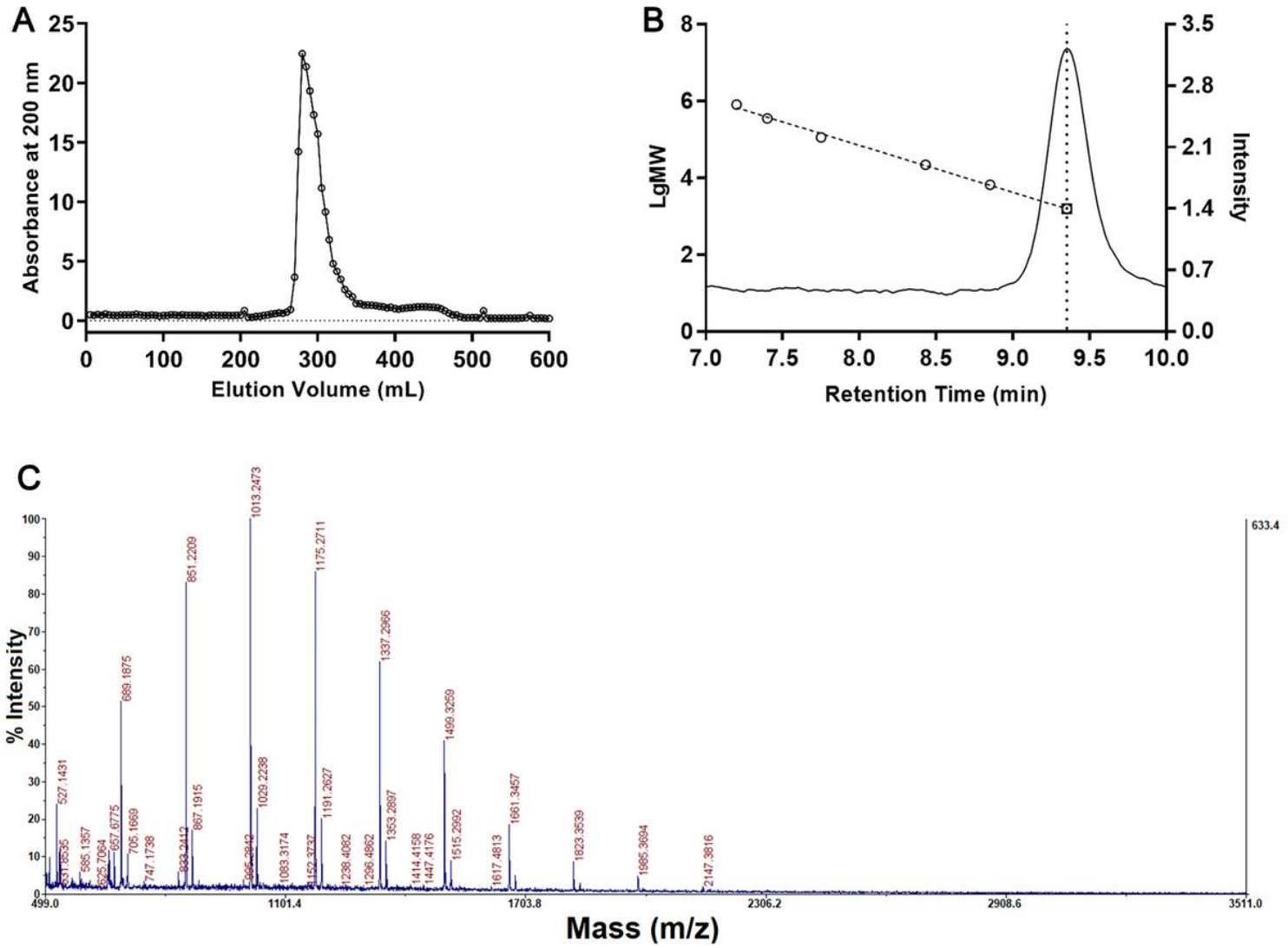

Figure 1

Purification and molecular weight characterization of AssP. A, the extracted AssP was concentrated and purified on a S-400 HR gel filtration chromatography column. Each 5 mL of elution was collected, and the content of total carbohydrate in each fraction was monitored by its absorbance at 200 nm. B, gel permeation chromatogram of the polysaccharide standards (not shown) and purified AssP (right y axis). The retention time and log value of molecular standards (empty circles) regressed into a linear relationship with a R2 value of 0.99338 (left axis). The retention time of AssP (dotted line vertical to the x-axis) corresponds to a molecule weight of 1543Da (empty square, intercept with the standard curve). C, MALDI-TOF/TOF mass spectrum of purified AssP.

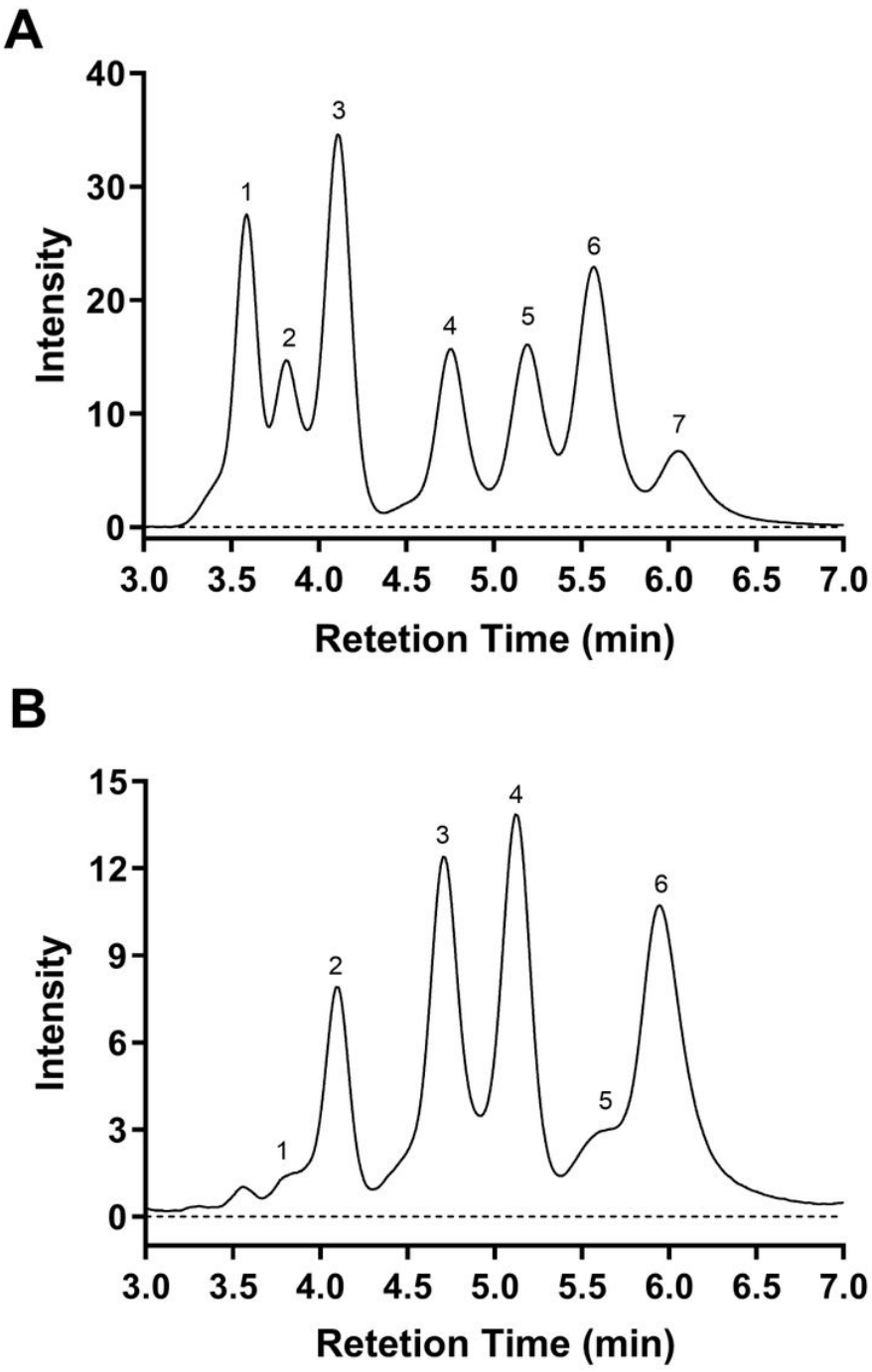

Figure 2

Monosaccharide composition of AssP. A, chromatogram of monosaccharide standard: 1, galactosamine; 2, rhamnose; 3, arabinose; 4, galactose; 5, glucose; 6, mannose; 7, fructose. B, chromatogram of Assp with peak identity:1, rhamnose; 2, arabinose; 3, galactose; 4, glucose; 5, mannose; 6, fructose.

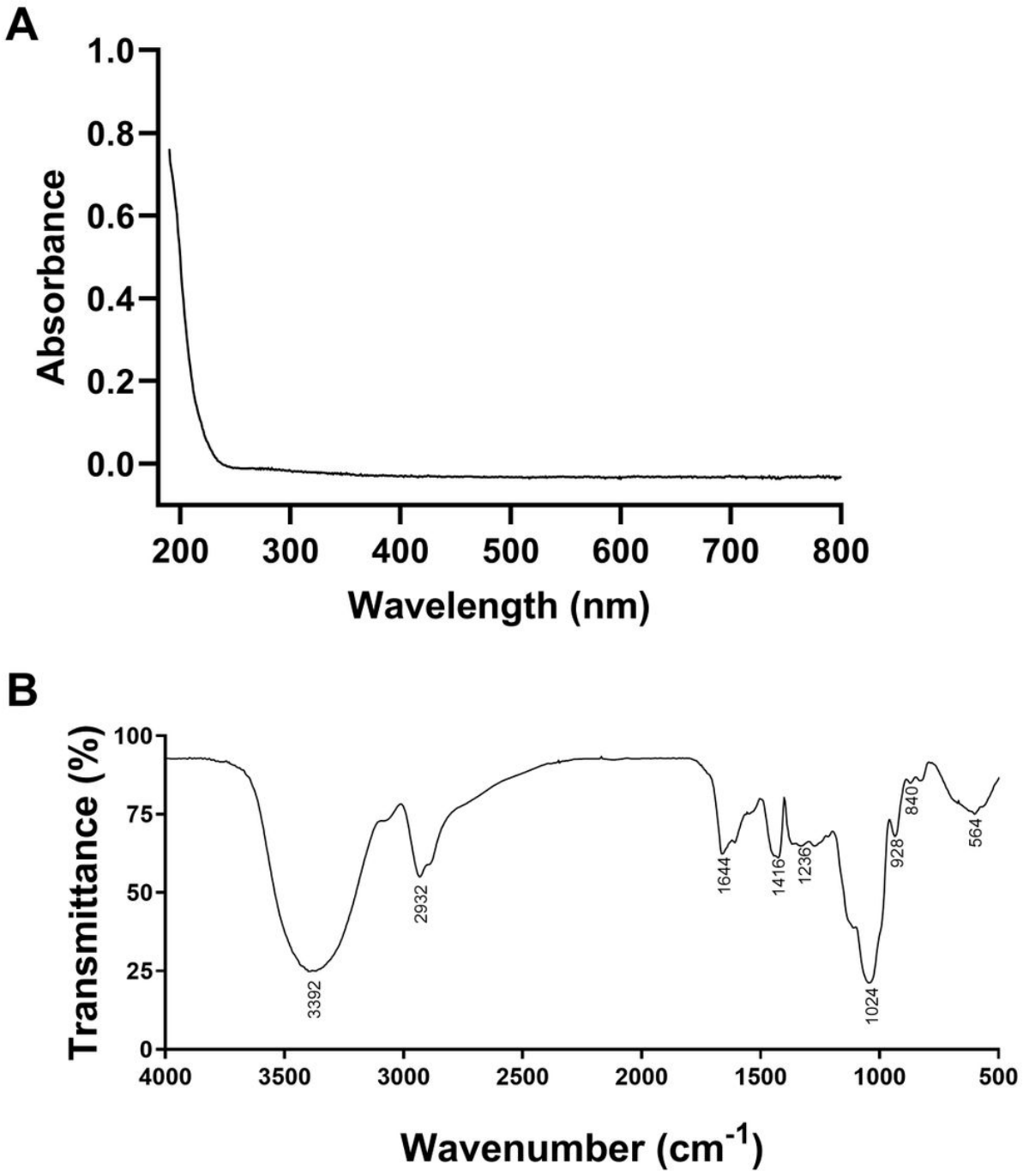

Figure 3

UV-Vis and FT-IR spectrums of AssP. A, the UV-Vis spectrum of an AssP water solution from 190-800 nm. B, the transmittance of AssP mixed with KBr on a FT-IR spectrometer of 500-4000 cm-1.

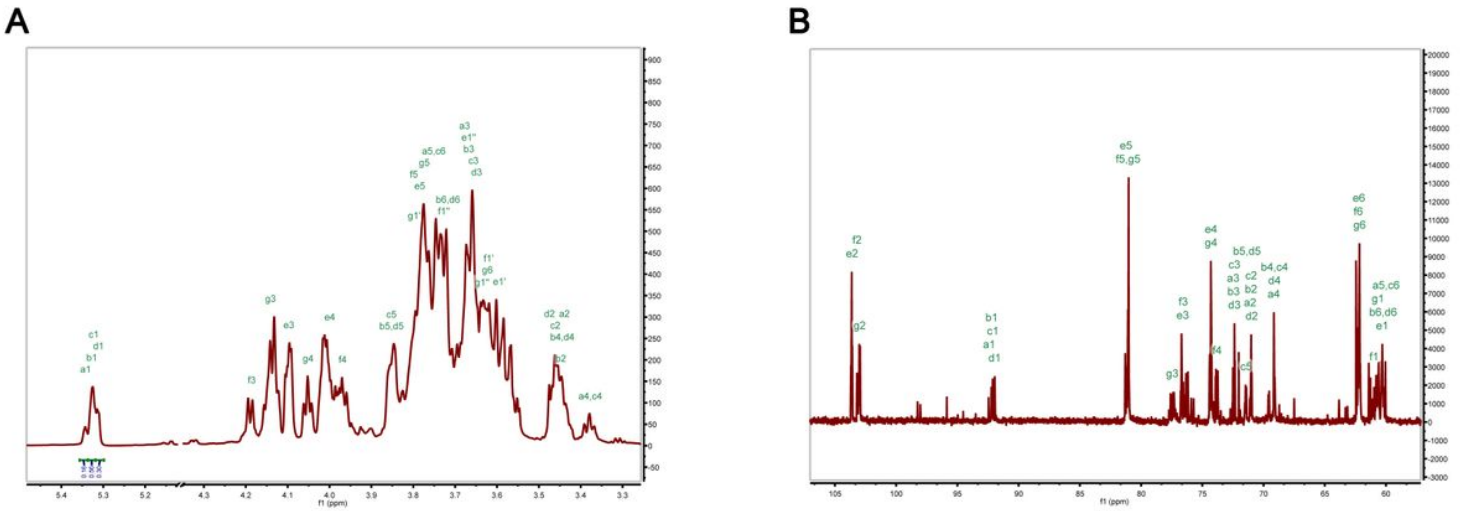

Figure 4

One dimensional NMR spectroscopy of AssP. One dimensional proton (A) and 13C (B) spectroscopy of deuterated AssP dissolved in D2O. The chemical shift of protons in AssP was recorded from 3.3 to 5.5 ppm and that of 13C was recorded from 50 to 107 ppm

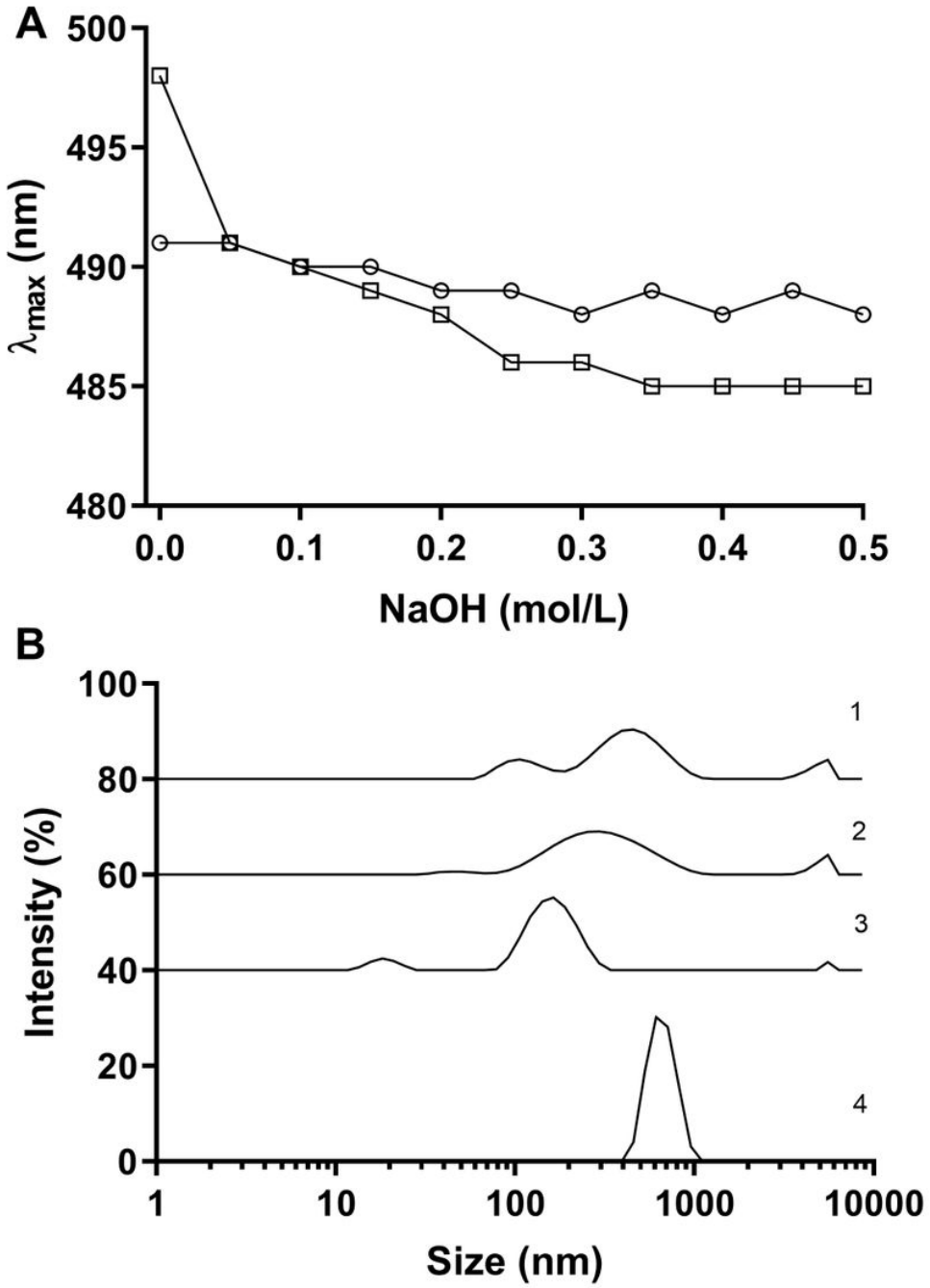

Figure 5

Tertiary structure characterization of AssP. A, the maximum absorbance wavelength of Congo-red (square) and Congo-red AssP mixture (circle) solution as the NaOH concentration changes. B, the dynamic light scattering intensity of AssP solution as a function of cumulative mean diameter at each purification step:1, water extraction, 2, after ethanol precipitation, 3, after pectin removal, 4, after gel filtration purification.

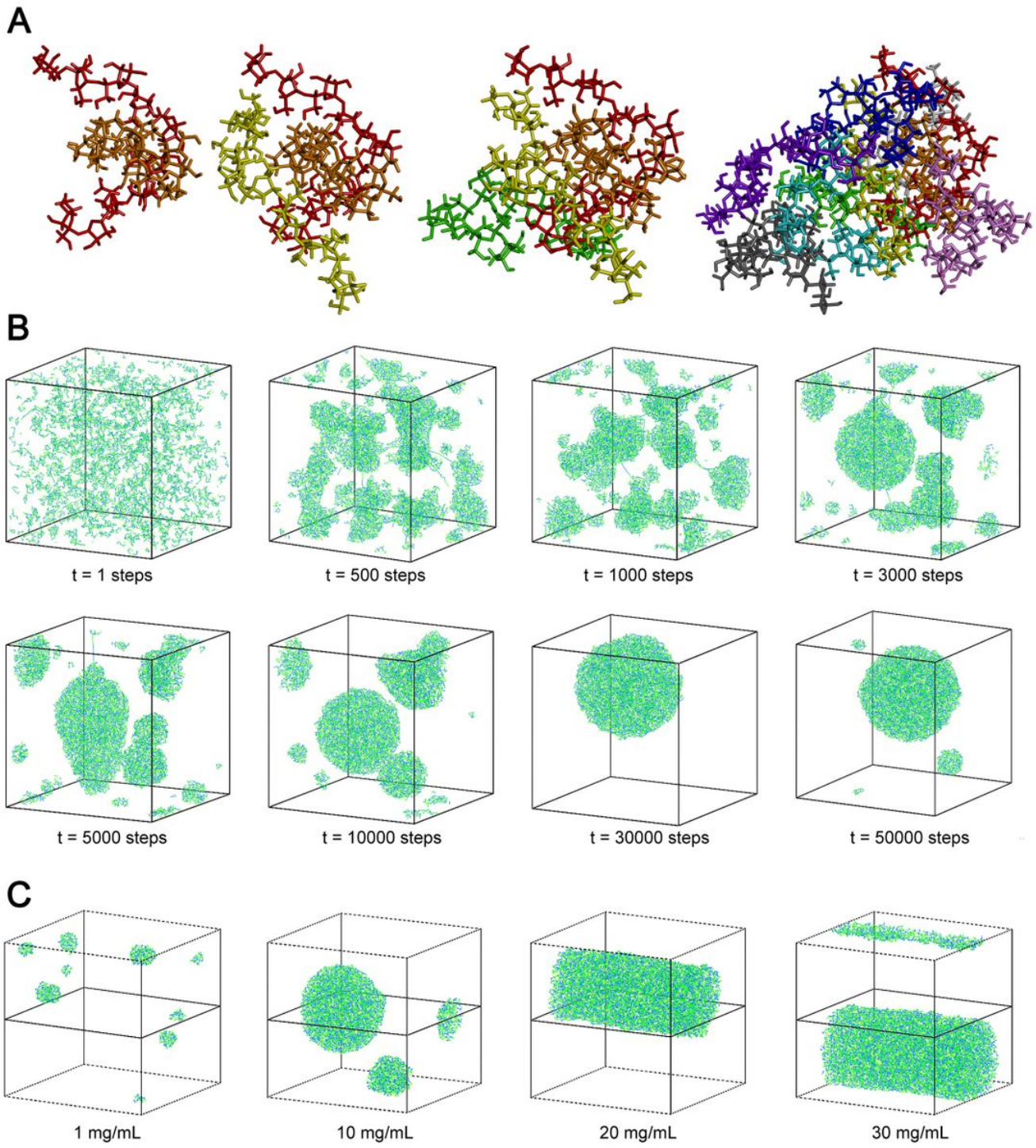

Figure 6

Simulation of AssP interactions and its solution behavior. A, the conformation of AssP and simulation of interactions between two, three, four and ten AssP molecules. The first AssP molecule in a horseshoe shape (red) was bound with a second one (orange). Sequential binding of the third one (yellow) and the forth one (green) are all involved in the direct interaction with the first AssP molecule. The following fifth (cyan), sixth (blue), seventh (purple), eight (white), ninth (black), and tenth (light purple) AssP molecule all binds to the preformed nuclei with a growth direction. B, the simulation of solution behavior of AssP molecules over time. C, the simulation of equilibrium solution state of AssP molecules at different concentrations.

Supplementary Files

This is a list of supplementary files associated with this preprint. Click to download.

- SupplementaryInformation.docx
- SupplementaryInformation.docx
- GraphicAbstract.tif
- GraphicAbstract.tif